Theory of Acoustic Propagation in 3 Dimensional Wedge Domain

3차원 쐐기형 영역에서의 음향파 전달 이론

Woo Jae Seong*
성 우 제*

ABSTRACT

Three components contribute to the acoustic field propagating in a wedge or over a ridge : a direct path arrival, an image component due to reflection from the boundaries and a component diffracted by the apex. All three contributions are included in a new, exact solution of the Helmholtz equation for the three-dimensional time harmonic field from a point source in a wedge(or over a ridge) formed by two intersecting, pressure-release plane boundaries. The solution is obtained by applying three integral transforms, and consists of an infinite sum of uncoupled normal modes. The mode coefficients are given by a finite integral involving a Gegenbauer polynomial in the integrand, which may be computed relatively efficiently. Results of the theory for propagation over a 90 degree ridge is discussed.

요 약

쐐기형 영역에서 전파되는 음향파는 다음 3가지 성분으로 분류할 수 있다 : 직접 전달 경로에 의한 성분, 경계면으로 부터의 반사에 의한 상(image) 성분 그리고 정점에 의한 산란 성분. 2개의 평면으로 경계가 구성된 쐐기(또는 봉우리) 영역에서 점원에 의한 3차원적인 시간 조화 장(field)에 대한 Helmholtz 방정식의 새로운 해를 구하였으며, 그 해는 위의 3가지 성분을 모두 내포하고 있다. 이 해는 정상모우드 들의 무한 급수로 이루어졌으며 각 모우드 계수는 Gegenbauer polynomial을 포함하는 유한적분으로 주어진다. 위의 해석해를 사용하여 봉우리 영역에서 음파의 분포를 계산하였다.

I. Introduction

In this paper an exact solution is developed for the acoustic field generated by a harmonic point source in an infinite wedge-shaped ocean, formed by two perfectly reflecting planes which intersect along the line of the apex. The new solution includes an image component of the field and a diffracted component arising from scattering at the apex, although emphasis is given in the discussion to the diffracted field since the normal modes associated with the image have been examined at length elsewhere[1]. The analysis is presented in the context of ocean wedges and ridges, but obviously has wider application.

It is well known that when the wedge angle θ_0 (Fig. 1a) is a submultiple of π(i.e. π divided by an

*Dept. Ocean Engineering, Inha University
인하대학교 선박해양공학과
접수일자 : 1994년 10월 21일

integer) there is no diffraction from the apex of the wedge[1, 2]. In general however, when the wedge angle is not a sub-multiple of π, diffraction from the apex does occur, although it may or may not be of significance. For a small wedge angle, say on the order of 2°(which is typical of the continental slope) diffraction effects are negligible even when θ_0 is not precisely a sub-mutiple of π. As the wedge angle increases, diffraction from the apex gains in significance, becoming a predominant factor when θ_0 exceeds π(Fig. 1b). Such large-angle wedges, with $\theta_0 > \pi$, are representative of the mid-ocean ridges and other ridge-like structures on the sea floor.

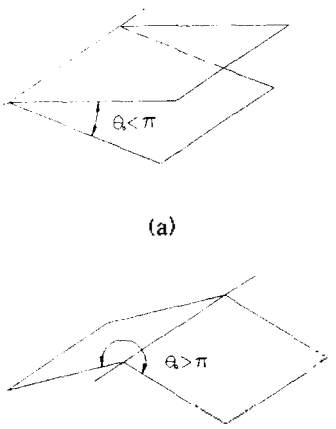

Figure 1. Schematic diagram for (a) wedge and (b) ridge problem.

Diffraction in wedges was first discussed by Sommerfeld[3] at the turn of the century. Since then an extensive literature has accumulated on acoustics and electromagnetics fields in wedge-like domains. In connection with acoustics, an exact solution in terms of normal modes was derived by Bradley and Hudimac[4] and examined by Graves et al[5]; and diffraction of a spherical transient by the apex of a wedge was addressed by Biot and Tolstoy[6] using the method of normal coordinates. Buckingham derived an exact solution for the case of a wedge void of diffraction component[1] and with diffraction component[7] which is expressed as an infinite integral. More recently, several numerical solutions of the wedge problems have appeared, based on the parabolic equation approximation[8], normal mode theory[9] and finite difference method[10]. However, these numerical methods are approximate solutions with inherent assumptions in the development stages or its implementation.

The starting point of the analysis presented here is the general expression for the field produced by a harmonic source in a perfect wedge derived by Buckingham[1]. This result, which is obtained from the inhomogeneous Helmholtz equation, is exact throughout the wedge-shaped domain including the source point. The solution is expressed in cylindrical coordinates(Fig. 2), with the z axis running along the apex of the wedge. As we shall show, the field consists of an image contribution (although image theory is not invoked in deriving the solution) and a diffracted component. By Fourier transforming our result for the CW field back into the time domain, it can be shown to be consistent with the impulsive field in a wedge derived by Biot and Tolstoy[6].

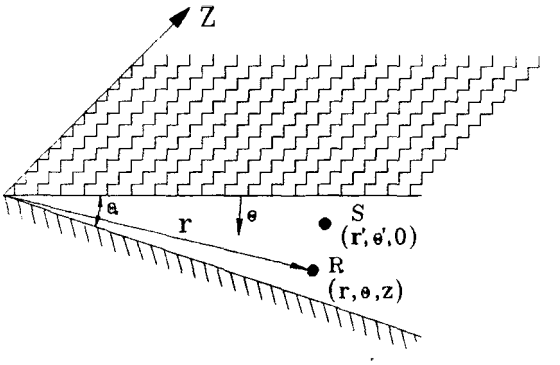

Figure 2. Cylindrical coordinate system.

II. The Time-Harmonic Field

When the wave equation with an impulsive source term is Fourier transformed with respect to time, it becomes the inhomogeneous Helmholtz equation :

$$\nabla^2\phi + k^2\phi = -Q\delta(\vec{r} - \vec{r}'), \tag{1}$$

where ∇^2 is the Laplacian, ϕ is the Fourier transform of the velocity potential of the fluid, k is the wavenumber, Q is the source strength, δ is the Dirac delta function, and $\vec{r}$ and $\vec{r}'$ are the receiver and the source points, respectively. For the case of a wedge with two perfectly reflecting boundaries, an exact solution for ϕ can be obtained in the form of a sum of normal modes. This solution has been derived in Ref.[1] for a wedge with pressure-release boundaries. A cylindrical coordinate system is used with z axis running along the apex of the wedge as illustrated in Fig. 2. On applying a sequence of three integral transforms (a finite Fourier sine transform over angular depth θ, a Hankel transform over range r, and a Laplace transform over cross-range z) to Eq. 1 a triply transformed version of the field is obtained. The field itself is then found by taking the corresponding three inverse transforms. The final result is

$$\phi = \frac{Q}{\theta_0} \sum_{\nu} I_\nu(r, r', z, \omega) \sin\nu\theta \sin\nu\theta', \tag{2}$$

where θ_0 is the wedge angle, ω is the angular frequency, (r, θ, z) are the receiver coordinates and $(r', \theta', 0)$ are the source coordinates and we set

$$\nu = \frac{m\pi}{\theta_0}, \qquad m = 1, 2, 3, \cdots \tag{3}$$

where m is the mode number, and the summation in Eq.2 is over all values of m. The mode coefficient I_ν is a function of range and cross-range, but not of angular depth, since this has been separated out and appears only in the eigenfunctions. I_ν is given by the infinite integral

$$I_\nu(r, r', z, \omega) = i \int_0^\infty p \frac{e^{i\eta|z|}}{\eta} J_\nu(pr) J_\nu(pr') dp \tag{4}$$

where $i = \sqrt{-1}$, J_ν is the Bessel function of the first kind of order ν and

$$\eta = \sqrt{k^2 - p^2}. \tag{5}$$

The wavenumber k is defined as $k = \omega/C$, with C the speed of sound in the medium contained in the wedge.

Eqs. 2 and 4 for the time harmonic field are exact, and valid for any wedge angle. Thus, this solution includes both the image component and the diffracted component of the time-harmonic field. The field due to an impulsive source is found by taking the inverse Fourier transform of Eq. 2. This involves an inversion integral over angular frequency, ω, which is a known form[11] :

$$\frac{1}{2\pi} \int_{-\infty}^{\infty} \frac{1}{\eta} e^{i\eta|z|} e^{i\omega t} d\omega = iCu(t - z/C) J_0(p\sqrt{C^2t^2 - z^2}), \tag{6}$$

where u is the unit step function. With the aid of this result, the transient field in the wedge can be expressed as

$$\phi = \frac{Q}{\theta_0} \sum_{\nu} \tilde{I}_\nu(r, r', z, t) \sin\nu\theta \sin\nu\theta', \tag{7}$$

where ϕ is the velocity potential of the field generated by the impulsive source, and

$$\tilde{I}_\nu(r, r', z, t) = -Cu(t - z/C) \int_0^\infty pJ_0(p\sqrt{C^2t^2 - z^2}) J_\nu(pr) J_\nu(pr'). \tag{8}$$

Eqs. 7 and 8 are exactly the same as the result for the transient field derived by Biot and Tolstoy [6] using the method of normal coordinates (except that their eigenfunctions are cosines rather that sines, because they considered the case of rigid boundaries). Since the properties of Eqs. 7

and 8 for the impulsive field have been explored fully in Ref. 6] they will not be further discussed here.

The tigonometric eigenfuntions in Eq. 2, representing the modes in the wedge, are shown for $m=1, 2, 3$ in Fig. 3. The number of extrema in each mode function is equal to the mode number, m. Note that the surfaces of constant phase are cylinders which are coaxial with the apex of the wedge. An elegant tank experiment recently reported by Tindle et al[12] confirmed that such cylindrical wavefronts are indeed observed in practice.

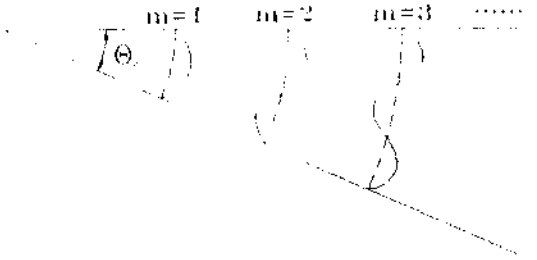

Figure 3. Mode shapes in angular direction for the first three modes.

The entire range and closs-range dependence of each of the modes is given by the mode coefficient equation. This coefficient for the time-harmonic field given by the integral in Eq. 4, has been examined in detail in Ref.[1] for wedge angles which are sub-multiples of π (*i.e.* ν an integer). This condition corresponds to the case where only the image component of the field is present, the diffracted component being identically zero. Central to the analysis was the transform of the infinite integral on Eq. 4 to a finite integral, using the Bessel function identity[13]

$$J_\nu(pr)J_\nu(pr') = \frac{1}{\pi}\int_0^\pi J_0(p\sqrt{r^2+r'^2-2rr'\cos\sigma})\cos(\nu\sigma)\,d\sigma. \tag{9}$$

This identity, derived from one of the Bessel function addition theorem, is valid only when ν is an integer. Thus, the convertion from an infinite to a finite integral in Ref.[1] was the mathematical process that excluded the diffracted field from the analysis. If the diffracted field is to be included, that is if ν is permitted to be fractional, Eq. 9 must be abandoned in favor of a more general formulation.

Ⅲ. Generalized Analysis of the Field

Eqs. 2 and 4 represent a complete, exact solution for the time-harmonic field in the wedge for any wedge angle. The depth dependence represented by the eigenfunctions is straightforward, but the infinite integral for the mode coefficients in Eq. 4 is not tractable and does not provide much physical insight into the (r, z) dependence of the field. In the following analysis, we convert this integral to another form which is more manageable, using an argument which is a generalized version of that used in Ref.[1] for the case of ν an integer.

We begin by writing the order of the Bessel functions in the integrand of Eq. 4 as the sum of an integer, n and a fraction, μ:

$$\nu = \frac{m\pi}{\theta_0} = n+\mu. \tag{10}$$

Then for unrestricted real values of ν, the Bessel function product in the integrand of the mode coefficient integral is given by the following identity[13]

$$J_\nu(pr)J_\nu(pr') = \frac{n!\,\Gamma(\mu)(pr)^\mu(pr')^\mu}{\pi 2^{1-\mu}\Gamma(n+2\mu)} \int_0^\pi \frac{J_\nu(pR_1)}{R_1^\mu}\,C_n^\mu(\cos\sigma)\sin^{2\mu}\sigma\,d\sigma, \tag{11}$$

where Γ is the gamma function, $C_n^\mu(\cos\sigma)$ is the Gegenbauer polynomial and

$$R_1 = \sqrt{r^2+r'^2-2rr'\cos\sigma}. \tag{12}$$

When the term on the right of Eq. 11 is substi-

tute into Eq. 4, the expression for I_ν takes the form of a double integral. One of these integrals, over an infinite range of the variable p, is as follows:

$$\int_0^\infty p^{\mu+1}\frac{e^{i\eta|z|}}{\eta}J_\mu(pR_1)dp. \tag{13}$$

On expanding the exponential function in the integrand in terms of the modified Bessel function $K_{\frac{1}{2}}$, this integral becomes a known form[13]. The eventual result for the mode coefficient is

$$I_\nu=-\sqrt{\frac{1}{8\pi}}\frac{n!\Gamma(\mu)}{\Gamma(n+2\mu)}(2rr')^\mu k^{\mu+\frac{1}{2}}\int_0^\pi \frac{H^{(2)}_{\mu+\frac{1}{2}}(kR_2)}{R_2^{\mu+1/2}}C_n^\mu(\cos\sigma)\sin^{2\mu}\sigma d\sigma, \tag{14}$$

where $H^{(2)}_{\mu+\frac{1}{2}}$ is the Hankel function of the second kind of order $\mu+\frac{1}{2}$. The parameter R_2 appearing in the integrand is given by

$$R_2=R_0\sqrt{1-2a\cos\sigma}$$

$$R_0=\sqrt{r^2+r'^2+z^2} \tag{15}$$

$$a=\frac{rr'}{R_0^2}.$$

Eq. 14 is an exact expression for the mode coefficient I_ν, involving a finite integral rather than an infinite integral as in Eq. 4. By using the limiting relationship

$$\lim_{\mu\to 0}\Gamma(\mu)(\mu+n)C_n^\mu(\cos\sigma)=2\cos n\sigma, \tag{16}$$

it is fairly easy to show that when $\mu\to 0$, Eq. 14 reduces to

$$\lim_{\mu\to 0}I_\nu=\frac{1}{\pi}\int_0^\pi \cos n\sigma\frac{e^{-ikR_2}}{R_2}d\sigma, \tag{17}$$

which is the correct result for wedge angles which are submultiples of π. Eq. 17 represents the field in the wedge due to a finite number of images. It shows distinctive features in the (r, z) plane which are due to horizontal refraction caused by repeated reflections from the inclined boundaries of the waveguide. These features include acoustic shadowing in the horizontal and intra-mode interference [14, 15].

Returning now to Eq. 14, we see that the integrand contains a Hankel function of low order ($|\mu+1/2|\leq 1$), and the Gegenbauer polynomial $C_n^\mu(\cos\sigma)$, it is convenient to replace the latter by the following finite series[16]:

$$C_n^\mu(\cos\sigma)=\sum_{m=0}^{n}\frac{\Gamma(\mu+m)\Gamma(\mu+n-m)}{\Gamma^2(\mu)m!(n-m)!}\cos(n-2m)\sigma. \tag{18}$$

Using the expression to evaluate the Gegenbauer polynomials, the mode coefficient in Eq. 14 can be computed efficiently. By performing the mode sum in Eq. 2 the full harmonic field in the wedge may be calculated exactly.

Ⅳ. Numerical Examples

We shall primarily look at the total field behavior when the wedge angle is not a submultiple of π. First, the dependence of the total field, which includes the diffraction component, along the range and apex direction will be shown. Then the angular dependence of the field will be investigated for the case when $\theta_0=\frac{3}{2}\pi$ (ridge case).

The dependence of the field along the radial direction, when other parameters are fixed, will exhibit a decay inversely proportional to $|r-r'|$ as can be seen from Eq. 14. Fig. 4 shows the magnitude of the mode coefficient, $|I_\nu|$, for the first mode when $\theta_0=\frac{3}{2}\pi$, $k=1.0$, $z=0$ and $r'=1000$ (m). The field decaying away from the source point at $r=1000$(m) is evident and the field is increased in the vicinity of the apex which is due to the diffracted component. Due to the interaction of diffracted wave propagating away from the apex and the wave originating from the source

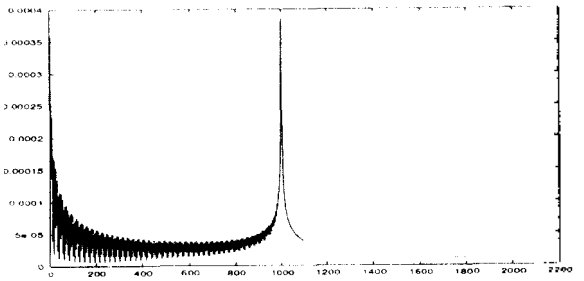

Figure 4. Field variation along the radial direction for a ridge problem. $\theta_0 = 270^\circ$, $k = 1$, $r' = 1 \times 10^5$, $z = 0$.

which is propagating towards the apex, the oscillating field is generated within the sector between the apex and the source. Beyond that sector, the interaction of both waves which happen to propagate in coherent direction produces smooth fields. The mode coefficients for other modes will be similar to that of the first mode.

The field variation along cross range, when source and receiver ranges are fixed, reflects the modal butterfly pattern for all wedge angles. This is due to the refraction of rays as they reflect off the boundary surfaces of the wedge. Fig. 5 show the magnitude of the mode coefficient, $\pi R_0 |I_\nu|$, for the 1st mode when the wedge angles are 2° and 2.01°, respectively. Other parameters are shown in the figure. When the wedge angle is small, the diffracted component is seen to be of negligible amount as can be seen from the comparison of the two and the field decays quite rapidly above the caustic point. There is a little difference of the field near $z = 0$ point due do the diffracted component. Fig. 6 shows the modal butterflies for modes 1, 2, 3 and 4 for the case of a ridge with $\theta_0 = \frac{3}{2}\pi$. The field decay beyond the caustic is procrastinated due to void of refraction when the wedge angle becomes larger than π.

The angular dependence of the field by a ridge with an external angle of $\theta_0 = \frac{3}{2}\pi$ is given as a final example. The acoustic field is calculated from Eqs. 2, 14 and 18. The results are shown as polar

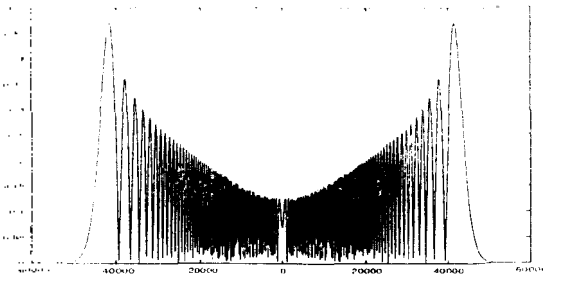

(a)

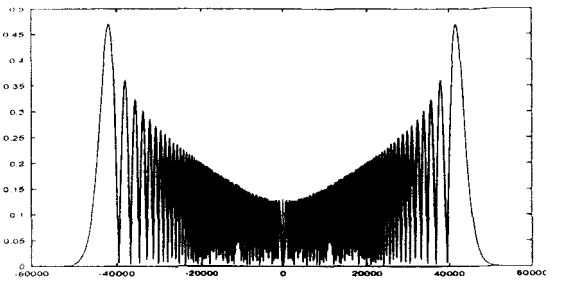

(b)

Figure 5. Field variation along the shoreline direction for a wedge problem. $k = 1$, $r = 1 \times 10^4$, $r' = 400$. (a) $\theta_0 = 2^\circ$ and (b) $\theta_0 = 2.01^\circ$.

diagrams for the absolute value of the velocity potential, $|\phi|$, as a function of angular depth of the receiver θ. Fig. 7 shows the field over a ridge for four source positions. The fixed parameters are as follows : $k = 1\text{m}^{-1}$, $r = 400\text{m}$, $r' = 10{,}000\text{m}$ and $z = 5000\text{m}$. Since larger angles support more modes six hundred modes were used in the computation of the field. The field containing reflected components shows very sharp peaks and troughs, whilst the region with direct and diffracted components is somewhat smoother, with broader peaks and shallower troughs. Due to relatively high wavenumber, the diffracted component is almost negligible in this case. When $k = 1.0 \times 10^{-4}\text{m}^{-1}$, $r = 10\text{m}$, $r' = 100\text{m}$ and $z = 0\text{m}$ (Fig. 8), the difrracted component becomes noticeable. 10 modes were used altogether for the computation of the field.

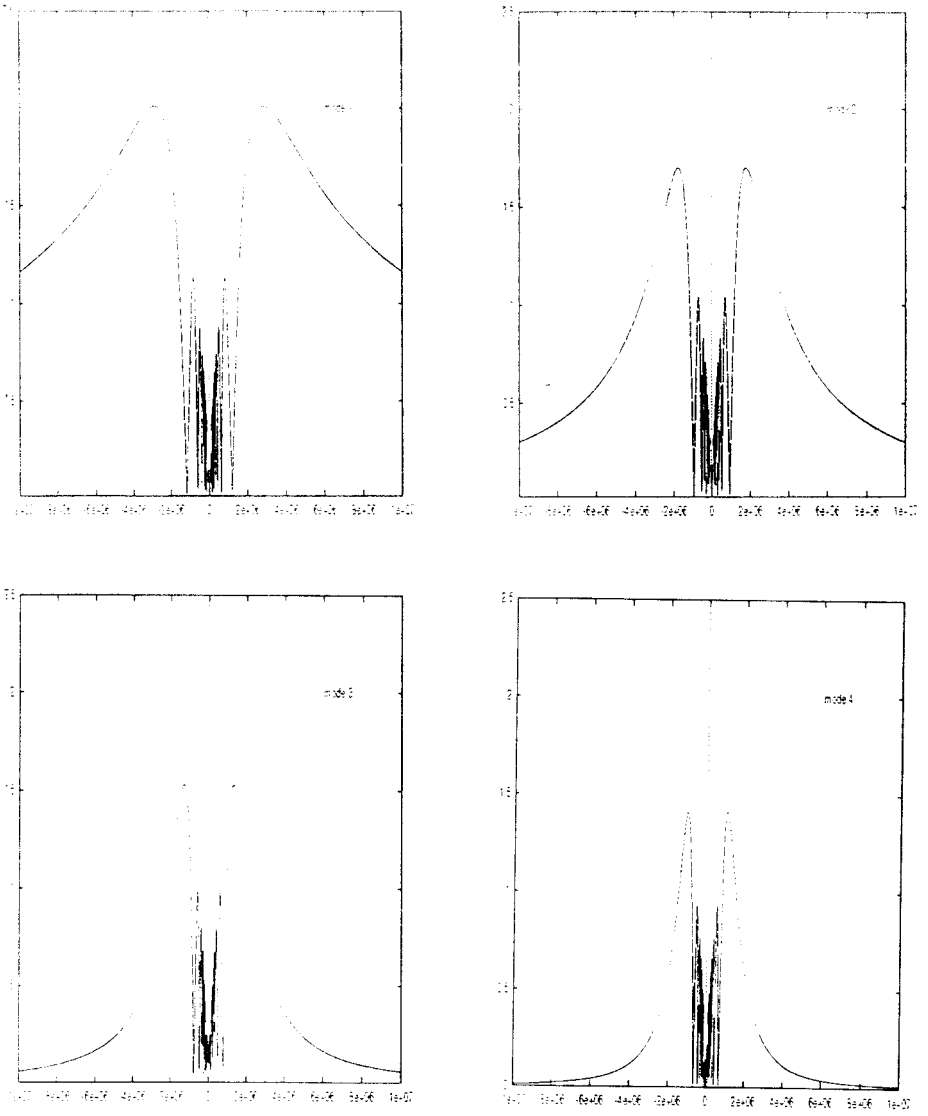

Figure 6. Field variation along the apex direction for the first 4 modes in a ridge problem. $\theta_0 = 270°$, $k = 1$, $r = 1 \times 10^1$, $r' = 400$.

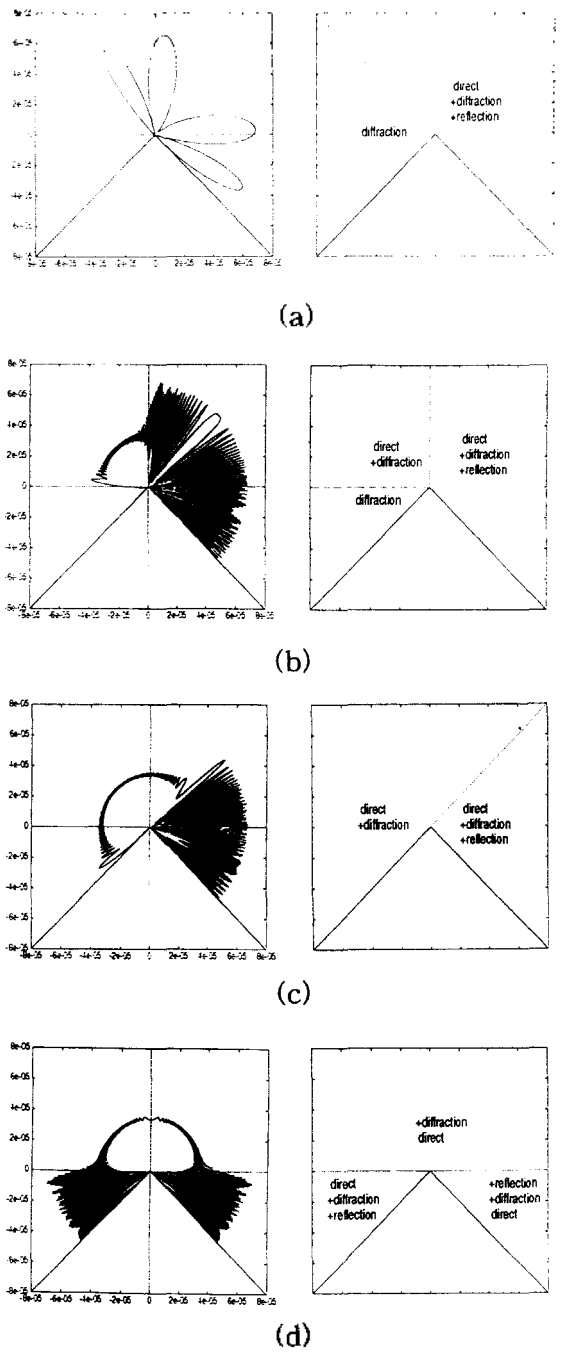

Figure 7. Polar diagram of the field for four different source positions when $\theta_0 = 270°$, $k = 1$, $r = 400$, $r' = 1 \times 10^4$, $z = 5 \times 10^3$: (a) $\theta' = 1°$, (b) $\theta' = 45°$, (c) $\theta' = 90°$ and (d) $\theta' = 135°$. The small diagram to the right shows the components that contribute to the total field in different sectors. The asterisk indicates the source position.

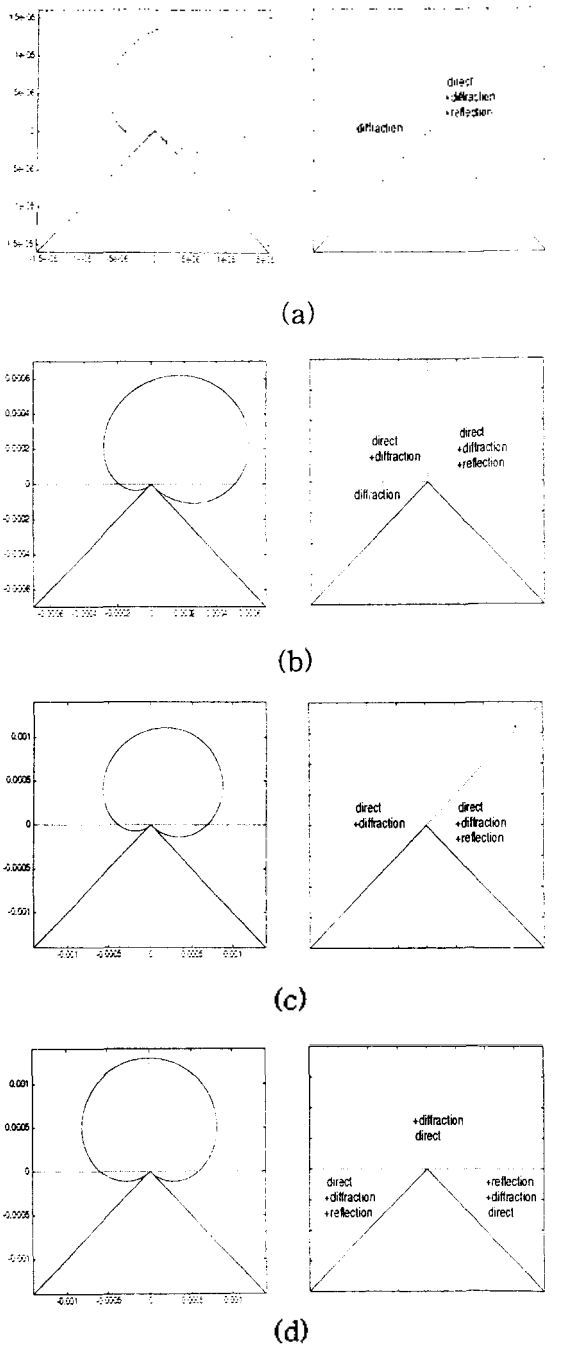

Figure 8. Polar diagram of the field for four different source positions when $\theta_0 = 270°$, $k = 1 \times 10^4$, $r = 10$, $r' = 100$, $z = 0$: (a) $\theta' = 1°$, (b) $\theta' = 45°$, (c) $\theta' = 90°$ and (d) $\theta' = 135°$.

V. Summary and Conclusion

The theory presented above gives the total field in a wedge or over a ridge due to a time-harmonic point source. The final expression for the field consists of an infinite sum of normal modes. It is *exact*, involving no approximation, where the mode coefficients are expressed as a finite integral involving Hankel functions and Gegenbauer polynomials.

In ocean acoustics, the theory described above may find application in connection with propagation over ridge-like seamounts, where scattering from the apex is significant. It may also be relevant to the problem of acoustic scattering from the ice canopy in the arctic ocean, since ice keels of various dimensions, resembling inverted ridges, are a characteristic feature of the ice.

References

1. M. J. Buckingham, "Acoustic propagation in a wedge-shaped ocean with perfectly reflecting boundaries," in *Hybrid Formulation of Wave Propagation and Scattering*, edited by L. B. Felsen (1984).
2. J. B. Keller, "The scope of the image method," *Comm. Pure Appl. Math.* 6 : 505-512 (1953).
3. A. Sommerfeld, "Mathematische theorie der diffraction," *Math. Ann.* 47 : 317-374 (1896).
4. D. L. Bradley and A. A. Hudimac, "The propagation of sound in a wedge shaped shallow duct," *Nav. Ord. Lab. Rep.* NORTR 70-235, (1970).
5. R. D. Graves, A. Nagl, H. Uberall and G. L. Zarur, "Range-dependent normal modes in underwater sound propagation : application to the wedge shaped ocean," *J. Acous. Soc. Am.* 58 : 1171-1177 (1975).
6. M. A. Biot and I. Tolstoy, "Formulation of wave propagation in infinite media by normal coordinates with an application to diffraction," *J. Acous. Soc. Am.* 29 : 381-391 (1957).
7. M. J. Buckingham, "Theory of acoustic radiation in corners with homogeneous and mixed perfectly reflecting boundaries," *J. Acous. Soc. Am.* 86 : 2273-2291 (1989).
8. M. D. Collins, "Benchmark calculations for higher-order parabolic equations," *J. Acous. Soc. Am.* 87 : 1535-1538 (1990).
9. F. B. Jensen and C. M. Ferla, "Numerical solutions of range-dependent benchmark problems in ocean acoustics," *J. Acous. Soc. Am.* 87 : 1499-1510 (1990).
10. R. A. Stephen, "Solution to range-dependent benchmark problems by the finite-difference method," *J. Acous. Soc. Am.* 87 : 1527-1534 (1990).
11. I. S. Gradshteyn and I. M. Ryzhik, *Tables of Integrals, Series and Products*, Academic Press, New York (1980).
12. C. T. Tindle, H. Hobaek and T. G. Muir, "Downslope propagation of normal modes in a shallow water wedge," *J. Acous. Soc. Am.* 81 : 275-286 (1987).
13. G. N. Watson, *A Treatise on the Theory of Bessel Functions*, Cambridge University Press, Cambridge (1958).
14. C. H. Harrison, "Three dimensional ray paths in basins, troughs and near seamounts by use of ray invariants," *J. Acous. Soc. Am.* 62 : 1382-1388 (1977).
15. C. H. Harrison, "Acoustic shadow zone in the horizontal plane," *J. Acous. Soc. Am.* 65 : 56-61 (1979).
16. N. N. Lebedev, *Special Functions and their Applications*, Dover Publications, New York (1972).

▲成 宇 濤(Woojae Seong) 1960년 1월 6일생

1982년 2월 : 서울대학교 공과대학 조선공학과 졸업 (공학사)

1984년 2월 : 서울대학교 대학원 조선공학과(공학석사)

1991년 2월 : Dept. Ocean Engineering, M.I.T. (공학박사)

1992년 3월 ~ 현재 : 인하대학교 선박해양공학과 조교수